Phase diagram for stimulus-responsive materials containing dipolar colloidal particles

Amit Goyal, Carol K. Hall,* and Orlin D. Velev
Department of Chemical and Bimolecular Engineering, North Carolina State University, Raleigh, North Carolina, USA
(Received 9 April 2007; revised manuscript received 16 November 2007; published 3 March 2008)

Dipolar colloidal particles self-assemble into a rich variety of microstructures ranging from co-crystals of unusual symmetry, to open networks (gels) of cross-linked chains of particles. We use molecular dynamics computer simulation to explore the self-assembly, structure, crystallization and/or gelation of systems of colloid particles with permanent dipole moments immersed in a high-dielectric solvent. Particle-particle interactions are modeled with a discontinuous potential. The phase diagram in the temperature-packing fraction plane is calculated. Several types of phases are found in our simulations: ordered phases including face-centered-cubic, hexagonal-close-packed, and body-centered-tetragonal at high packing fractions, and fluid, string-fluid, and gel phases at low packing fractions. The very low volume fraction gel phases and the well-ordered crystal phases are promising for advanced materials applications.

DOI: 10.1103/PhysRevE.77.031401 PACS number(s): 64.60.−i, 64.75.Xc, 64.75.Yz, 64.70.Nd

Colloidal particles with directional interactions that self-assemble into predefined microstructures have the potential to serve as the foundation for the next generation of micro- and nanostructures with remarkable complexity and precision [1–7]. Suspensions of dipolar colloidal particles have attracted attention recently due to their tunable materials properties and their potential applications as storage media and display devices [4,5]. Dipolar colloids are ideal building blocks for the assembly of long-range ordered lattices such as colloidal crystals and gels and are being explored for many intriguing applications [8–12]. For example, two-dimensional (2D) crystals of dipolar colloids could be used as arrays of microlenses in image processing and photolithography [12]. Other technological applications for these advanced materials include smart ion-sensitive gels (solid at high salt concentration, liquid at low salt concentration), water-based electrorheological fluids and colloidal liquid crystals (LC) with improved properties for applications in displays, LC thermometers, and optical imaging.

Significant progress towards the practical fabrication of particles of anisotropic surface charge and composition has been made in the last few years. For example, Cayre *et al.* have developed a technique for preparing dipolar colloid particles by microcontact printing of films of ionic surfactants onto monolayers of colloid particles [13]. Other techniques for the preparation of anisotropic particles have been based on evaporation of gold on colloid monolayers [14], and on deposition of polymers on colloids using the Langmuir-Blodgett technique [15]. Velegol and coworkers have developed a particle lithography technique for fabricating colloidal doublets or microspheres with localized nanoscale charge distribution on the surface [16,17]. Granick and coworkers used an oil-water emulsion technique to synthesize two kinds of Janus colloidal particles—dipolar particles and particles that are charged on one side and hydrophobic on the other [18]. The experimental challenges of producing large quantities of monodispersed asymmetrically charged colloid particles and the multitude of possible structures that these particles can form make experimental study of all possible variations infeasible. Here we use computer simulation to explore the rich phase behavior (including formation, structure, crystallization and/or gelation) of materials containing dipolar colloid particles so as to guide the discovery of advanced materials in the laboratory.

Dipolar fluids have been the subject of many theory-based investigations. The phase diagrams for hard- and soft-sphere systems with *induced* dipole moments have been determined by Hynninen *et al.* using Monte Carlo simulations in the canonical ensemble (*NVT*) [19]. Since dipole-dipole interactions driven by external electric or magnetic fields favor orientations in which the dipoles align head to toe, the particles tend to form strings in the direction of the field. Hynninen *et al.* also showed that in the limit of high field, their system formed crystal phases including body-centered-tetragonal (bct) and hexagonal-close-packed (hcp). The crystal structures for fluids of spherical particles with an embedded point dipole modeled using a Stockmayer potential have been investigated by Groh and Dietrich using Monte Carlo simulations with Ewald summation [20,21]. They found three phases depending upon the value of the dipole moment: hexagonal, body-centered orthorhombic, and body-centered-tetragonal. Molecular dynamics simulations by Blaak *et al.* showed that dispersions of dumbbell-shaped, dipolar colloid particles undergo a gelation transition [22].

Safran *et al.* used percolation theory to study the topological properties of systems with thermoreversible crosslinks including gels, microemulsions, dipolar liquids, and colloids [23]. This work focused on the percolation transition, the point at which a network spanning the entire volume is formed. They found that a system of self-assembling branched chains passed through a percolation threshold at which a network spanning the entire volume was formed when the system packing fraction increased or the temperature decreased.

In this paper, we present the full phase diagram for systems of colloid particles with *permanent* dipole moments immersed in a high dielectric solvent. In the limit of zero dipole moment, hard-sphere phase behavior is recovered. At high dipole moments, several different types of phases are

*hall@eos.ncsu.edu

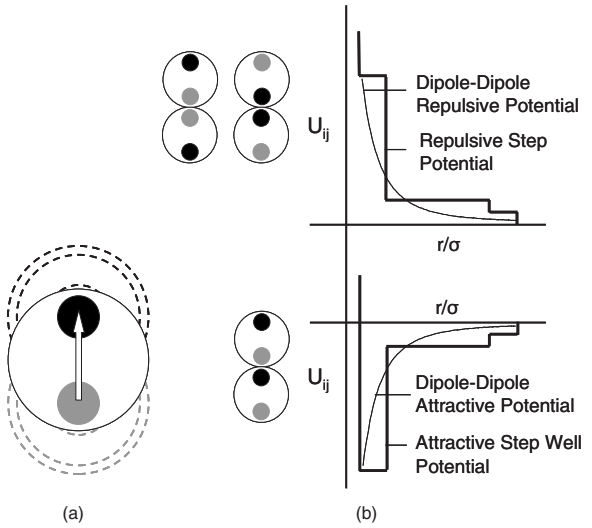

FIG. 1. Representation of dipolar particle. (a) Each sphere represents a dipolar particle with two oppositely charged small spheres embedded in it. (b) Spheres of like charge repel each other. Spheres of unlike charge attract each other.

found including fcc, hcp, and bct crystal phases at high packing fractions, and fluid, string-fluid, and gel phases at low packing fractions. We explore the effects of temperature, concentration, and dipole moment strength on the assembly process in order to obtain the full phase behavior. Interactions between dipolar particles are modeled using a discontinuous potential that retains the directional features of the forces responsible for self-assembly of dipolar colloid particles in high dielectric solvent but is not so detailed that the simulations become too computationally intensive. This potential, which is actually a potential of mean force since the solvent is modeled implicitly, well approximates the short-ranged orientational interactions which dominate the phase behavior. Long-ranged electrostatic interactions, which play an important role in vacuum, are not explicitly accounted for since these interactions are screened in a high dielectric solvent. Simulations of the self-assembly of these model particles are performed using discontinuous molecular dynamics (DMD) [24], a very rapid alternative to traditional molecular dynamics (MD), in which the forces on the particles are calculated only when discontinuities in the potential are encountered.

Each particle is modeled as a hard sphere with two oppositely charged small spheres embedded in it as shown in Fig. 1(a). The interactions between the like charge spheres are modeled using a three-step square shoulder repulsive potential and the interactions between the unlike charge spheres are modeled using a three-step square well attractive potential as shown in Fig. 1(b). The dashed lines in Fig. 1(a) represent the widths of the square shoulder and the square well.

The hard-sphere (U_{hs}), three-step square shoulder (U_{ss}), and three-step square well (U_{sw}) potentials are as follows:

$$U_{hs}(r_1) = \begin{cases} \infty & \text{if } r_1 < \sigma \\ 0 & \text{if } r_1 > \sigma \end{cases},$$

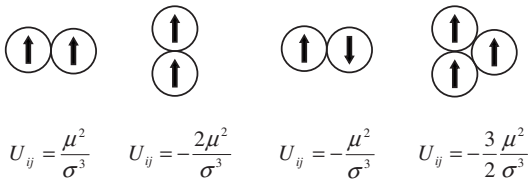

FIG. 2. Dipolar interaction energy, $U_{ij}=\frac{1}{r^3}(\vec{\mu}_i\cdot\vec{\mu}_j)-\frac{3}{r^5}(\vec{\mu}_i\cdot\vec{r}_{ij})\times(\vec{\mu}_j\cdot\vec{r}_{ij})$ between particles i and j for different configurations. The particles have dipole moment μ and diameter σ.

$$U_{ss}(r_2) = \begin{cases} \infty & \text{if } r_2 < \sigma_1 \\ \varepsilon_1 & \text{if } \sigma_1 < r_2 < (1+\lambda_1)\sigma_1 \\ \varepsilon_2 & \text{if } (1+\lambda_1)\sigma_1 < r_2 < (1+\lambda_2)\sigma_1 \\ \varepsilon_3 & \text{if } (1+\lambda_2)\sigma_1 < r_2 < (1+\lambda_3)\sigma_1 \\ 0 & \text{if } r_2 > (1+\lambda_3)\sigma_1 \end{cases},$$

$$U_{sw}(r_2) = \begin{cases} \infty & \text{if } r_2 < \sigma_1 \\ -\varepsilon_1 & \text{if } \sigma_1 < r_2 < (1+\lambda_1)\sigma_1 \\ -\varepsilon_2 & \text{if } (1+\lambda_1)\sigma_1 < r_2 < (1+\lambda_2)\sigma_1 \\ -\varepsilon_3 & \text{if } (1+\lambda_2)\sigma_1 < r_2 < (1+\lambda_3)\sigma_1 \\ 0 & \text{if } r_2 > (1+\lambda_3)\sigma_1 \end{cases},$$

where r_1 is the distance between colloidal particles, r_2 is the distance between embedded charged small spheres, σ is the colloidal particle diameter, $\sigma_1=0.3\sigma$ is the diameter of the small charged sphere, 0.6σ is the separation between charged small spheres on the same colloidal particle. The ε_1, ε_2, and ε_3 are the interaction energies between charged spheres and the λ_1, λ_2, and λ_3 are the widths of the square shoulder and square well. We chose a reference interaction strength of $\varepsilon^*=\mu^2/\sigma^3$ and will refer to the reduced parameters for the interaction strengths as $\varepsilon_1^*=\varepsilon_1/\varepsilon^*$, $\varepsilon_2^*=\varepsilon_2/\varepsilon^*$, and $\varepsilon_3^*=\varepsilon_3/\varepsilon^*$. The system packing fraction is defined as $\eta=\pi N\sigma^3/6V$, where V is the box volume and N is the number of colloid particles in the system. The reduced temperature is defined as $T^*=k_BT/\varepsilon^*$, where k_B is the Boltzmann constant and T is the temperature.

The dipole-dipole discontinuous potential is chosen to match standard expressions for the interaction energies, $U_{ij}=\frac{1}{r^3}(\vec{\mu}_i\cdot\vec{\mu}_j)-\frac{3}{r^5}(\vec{\mu}_i\cdot\vec{r}_{ij})(\vec{\mu}_j\cdot\vec{r}_{ij})$ between dipolar particles i and j when they are in the configurations shown in Fig. 2. The values of the square shoulder and the square well width parameters are $\lambda_1=0.500$, $\lambda_2=1.887$, $\lambda_3=2.333$ and the values of the interaction energy parameters are $\varepsilon_1^*=2.000$, $\varepsilon_2^*=1.500$, $\varepsilon_3^*=0.333$.

Discontinuous molecular dynamics (DMD) [24] simulations are performed in the canonical ensemble on systems containing 864 particles in a cubic cell with periodic boundary conditions. In discontinuous molecular dynamics (DMD) simulation, particles collide when they arrive at a discontinuity in the potential, that is, the hard-sphere diameter or the square-well width. Between collisions, particles move with linear trajectories, making DMD simulations much faster than traditional molecular dynamics simulations with con-

tinuous potentials which require a small integration time step. The postcollision velocities of particles in DMD are found by solving the collision dynamics equations analytically. To simulate chains of spheres effectively, Rapaport introduced bonds between spheres by limiting the distance between adjacent beads to be between σ and $\sigma(1+\delta)$, where δ is the bond extension parameter [25]. Later, Bellemans modified this model so that the distance between adjacent spheres must lie between $\sigma(1-\delta/2)$ and $\sigma(1+\delta/2)$ which makes the average bond length equal to σ [26]. We used the Bellemans model in our simulations to ensure that the dipole always passes through the center of the colloid particle. The value of δ in our simulations is 0.04.

Since we are interested in simulating at constant temperature, we use discontinuous canonical molecular dynamics (DCMD) [27–29], an adaptation of the standard microcanonical ensemble DMD technique. The DCMD technique is based on Anderson's stochastic collision method [27] and involves stochastic interactions of the system particles with imaginary constant-temperature heat bath particles. We assume that the system is immersed in a constant-temperature heat bath containing imaginary "ghost" particles. The ghost particles stabilize the system temperature by colliding with the system particles, resulting in the reassignment of particles velocities according to a Maxwell-Boltzmann distribution about the required temperature. Details of the DCMD method have been described by Gulati *et al.* [28] and by Zhou *et al.* [29].

The shape and volume of the simulation box are allowed to change in order to accommodate structures with periodic spacing. This is accomplished using the box length search algorithm of Schultz *et al.* [30] which calculates the pressure in different directions and then changes the box lengths to values that minimize the free energy of the system while maintaining constant density. The reduced pressure (P^*) in our simulations is calculated using the virial theorem.

$$P^* = \frac{P\sigma^3}{k_B T} = \frac{N\sigma^3}{V} - \frac{\sigma^3 m \sum_{coll} \vec{r}_{ij} \cdot \Delta\vec{v}_j}{3Vk_B Tt},$$

where m is the mass of each particle, $\vec{r}_{ij}$ is the distance between colliding particles i and j, $\Delta\vec{v}_j = -\Delta\vec{v}_i$ is the velocity change for particle j, Σ_{coll} refers to a sum over all collisions, and t is the elapsed simulation time.

Several different types of phases are found in our simulations. The resulting phase diagram is plotted in the packing fraction (η) versus reduced temperature (T^*) plane in Fig. 3. At low packing fractions we observe fluid, string-fluid, and gel phases. Our finding of an isotropic fluid phase at low densities is consistent with the prediction of Sear [31]. Our observation of two fluid-fluid transitions is consistent with the simulation results by Camps *et al.* on dipolar hard spheres who stated that they found "at least one isotropic-fluid-isotropic-fluid transition, and possibly two" [32]. They did not locate the phase boundaries for the transitions. At very high temperatures, hard-sphere phase behavior (a transition from fluid at low packing fraction to fcc solid at high packing fraction) is recovered. At high packing fractions we find ordered phases including face-centered-cubic (fcc), hexagonal-close-packing (hcp) and body-centered-tetragonal (bct).

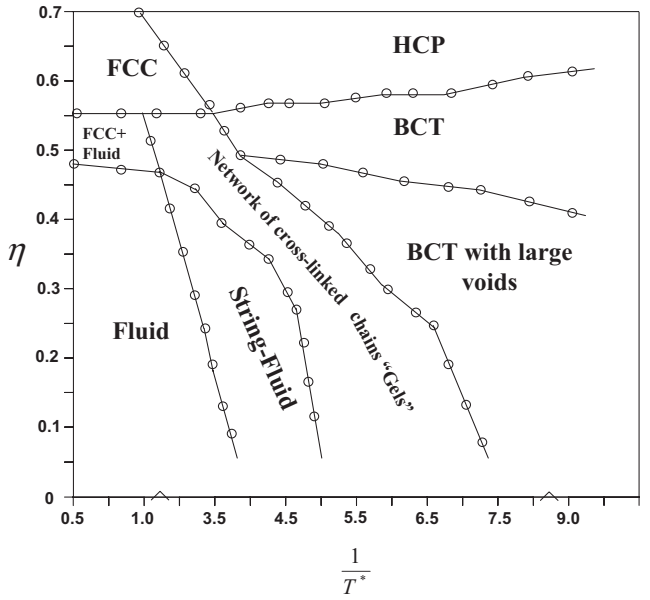

FIG. 3. Phase diagram for dipolar colloid particles in the packing fraction (η)—inverse temperature ($1/T^*$) plane.

To locate the transition between a fluid and a string-fluid, the average chain length distribution at different packing fractions, η for different reduced temperatures T^* is calculated. This is plotted in Fig. 4. The transition is defined to occur at the reduced temperature and packing fraction at which the average chain length, $\langle n \rangle$ increases dramatically. The average chain length drastically increases from three particles to approximately 30 particles at different packing fractions depending on the temperature, indicating that a sharp transition occurs between a fluid and a string-fluid at that packing fraction.

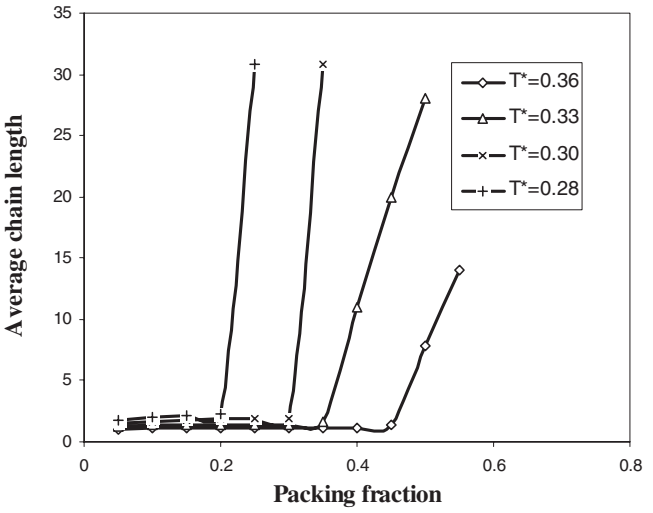

FIG. 4. Average chain length distribution at $T^*=0.28$, 0.30, 0.33, and 0.36 at different η values.

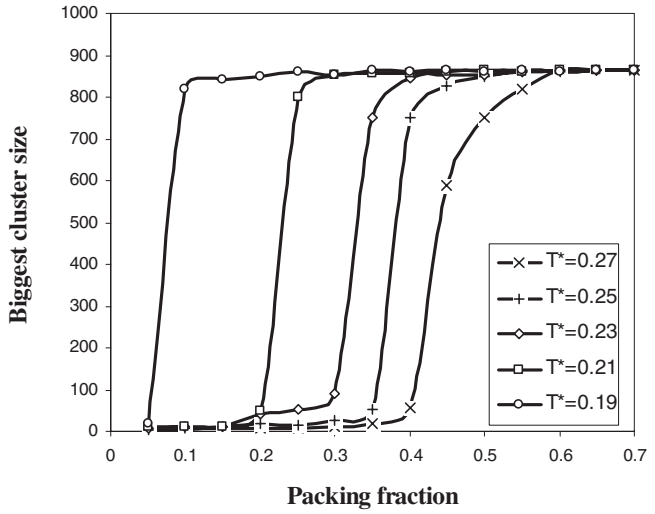

FIG. 5. Biggest cluster size versus packing fraction, η, at $T^*=0.19$, 0.21, 0.23, 0.25, and 0.27.

To locate the percolation transition between a string-fluid and a gel, the cluster size distribution at different packing fractions, η for different reduced temperatures, T^* is calculated [23]. The number of particles in a cluster is calculated as follows [34]. If the distance between particle A and particle B is smaller than the square-well width, we define particles A and B to be in the same cluster, say M_i. If we also find particles B and C in the same cluster, we then consider particles A, B, and C to be in the same cluster, M_i. Doing this for all particles in the system, we obtain a list of the particles in each cluster M_i and hence the number of particles in each cluster, the cluster size. A plot of the largest cluster size versus η is presented in Fig. 5. The string-fluid to gel transition is defined to occur at the reduced temperature and packing fraction at which the largest cluster size increases abruptly. The size of the largest cluster shows a rapid jump from five particles to approximately 840 particles at different packing fractions depending on the temperature, indicating a sharp percolation transition from a system with a large number of small clusters to a system with one big percolating cluster (a gel).

TABLE I. Values of the 3D bond orientational order parameters for some common 3D crystals [33].

Crystal	Q6	Q4	W6	W4
fcc	0.571	0.191	−0.013	−0.159
hcp	0.485	0.097	−0.012	0.134
bcc	0.511	0.036	0.013	0.159
icosahedral	0.663	0	−0.170	0
liquid	0	0	0	0

A series of snapshots of the system as temperature decreases through the string-fluid → gel transition at $\eta=0.10$ is illustrated in Fig. 6. The system is a string-fluid at $T^*=0.21$ and is a network of cross-linked chains at $T^*=0.19$; hence the percolation transition occurs between of $T^*=0.21$ and $T^*=0.19$. As temperature decreases from $T^*=0.19$ to $T^*=0.15$, pore size increases due to coarsening of the gel into thicker strands.

The hexagonal-close-packed (hcp), body-centered-tetragonal (bct), and face-centered-close-packed (fccp) crystal phases for the dipolar colloid particle systems are located by calculating the three-dimensional bond orientational order parameters Q and W. The 3D bond orientational parameters are sensitive to the degree of crystallinity in the system. To calculate these parameters, we use a method proposed by Steinhardt and coworkers [33] in which the type of packing in a crystal is identified by matching the values of the four parameters Q_4, Q_6, W_4, and W_6 to the standard values for common crystals presented in Table I. Figure 7 shows snapshots from our simulation of the arrangement of dipolar colloid particles in hcp and bct structures. The results indicate that the judicious choice of conditions could lead to the formation of very large crystals without defects and grain boundaries. Thus, the use of dipolar particles instead of microspheres may be the route to the formation of high quality colloidal arrays for photonic and optoelectronic applications.

A different feature of the phase diagram is the appearance of a percolated gel phase at intermediate temperatures and nearly all particle volume fractions. The gel phase found here has not been seen for the hard- and soft-sphere systems with

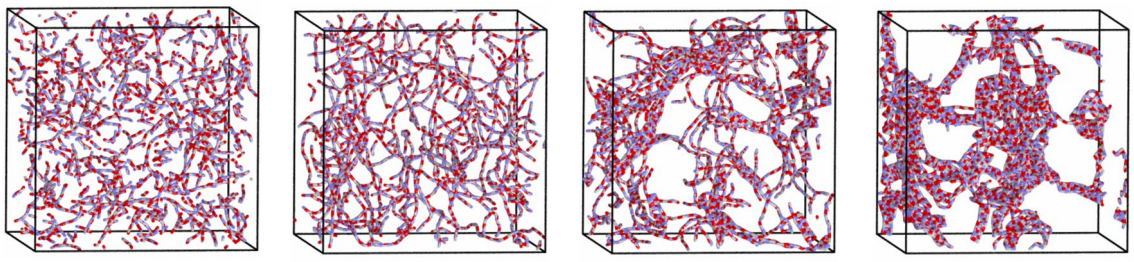

(a) String-Fluid (b) Gel with small pores (c) Gel with medium pores (d) Gel with large pores

Temperature decreases

FIG. 6. (Color online) Snapshot showing transition from fluid to gel-like open network at $\eta=0.1$ as temperature decreases. (a) $T^*=0.21$, (b) $T^*=0.19$, (c) $T^*=0.17$, and (d) $T^*=0.15$.

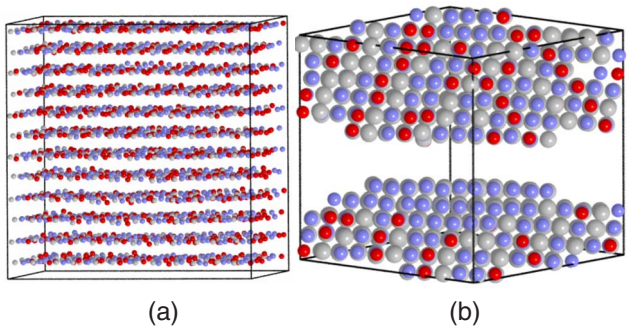

FIG. 7. (Color online) (a) Dipolar colloid particles packed hexagonally in each sheet with different sheets arranged in A-B-A-B-⋯-type hexagonal close packing. (b) Dipolar colloid particles arranged in body centered tetragonal structure.

induced dipole moments studied by Hynninen *et al.* [19]. The high propensity of the dipolar particles for gelation even at very low volume fractions can be attributed to the formation of dipolar chains by the particles. A further important aspect of the gelation process is the coarsening of the gel into thicker strands separated by large pores at low temperatures. This implies that the porosity, permeability, and mechanical stability of dipolar self-assembled particulate materials can be controlled by tuning the interactions and temperature. Characterizing the degree of porosity and designing a means to control materials properties will be the subject of a future publication.

In summary, we mapped out the phase behavior of colloid particles with permanent dipoles immersed in a high dielectric solvent in the temperature-packing fraction plane using molecular dynamics simulation. The discontinuous potential model used here describes Janus particles fairly accurately. Our results are in qualitative agreement with the results published by Sear [31], Camps *et al.* [32], and Hynninen *et al.* [19]. The most important aspect of our phase diagram that is also relevant for true dipolar systems is the appearance of a percolated gel phase at intermediate temperatures and nearly all particle volume fractions. The advantage of the discontinuous potential model presented here is that it allows for rapid evaluation of the possibilities for using dipolar colloidal particles in advanced materials applications based on phase behavior. It can easily be extended to more complex systems including binary mixtures of dipolar particles or quadrupolar particles. The disadvantages are that it does not consider multibody effects (meaning each dipole can only interact with one other dipole at a time) and is relatively short ranged compared to the $1/r^3$ potential in a true dipolar system. It mimics the actual dipolar interaction better at high densities than at low densities, hence our results are more accurate for dipolar systems at high densities than at low densities.

The question arises as to how our use of the stepwise potential affects our results and, in particular which aspects of our results are likely relevant for true dipolar systems. To answer this question we begin by pointing out that some of our phase boundaries—fluid to fcc+fluid, fcc+fluid to fcc, and bct with large voids to bct—were not calculated rigorously by either equating chemical potentials of two phases or locating a jump in an order parameter as we did for the fluid to string-fluid, string-fluid to gel, gel to bct with large voids, fcc to hcp, and hcp to bct phase transitions. Instead the phase boundaries—fluid to fcc+fluid, fcc+fluid to fcc, and bct with large voids to bct—were found by determining the density and temperature at which the type of structure present changed. A consequence of this approach is that the locations of the boundaries on either side of the fcc+fluid region may be less accurate than the other boundaries and the seemingly second-order phase transitions that we have drawn for the bct with large voids to bct may be first-order transitions. The question raised in 1993 by Caillol, "are the dipoles able to induce a liquid-gas transition in the dipolar hard sphere fluid?" [35] cannot be addressed in our simulations because we do not accurately account for the long range of the interaction. It is well known that increasing the range of a potential can cause a gas-liquid transition with a critical point that is metastable with respect to a solid-fluid transition to become stable, resulting in gas, liquid, and solid phases [36]. We have seen no evidence for a gas-liquid transition with a critical point within our fluid domain at moderate temperature. Evidence to date presented in the literature indicates that such a transition does not exist for dipolar hard spheres [37] although it has been seen for the Stockmayer fluid (Lennard Jones plus dipolar potential) [38]. Based on these observations we believe that even if we were better able to account for the long range of the dipole-dipole potential, we would not find a gas-liquid transition with a critical point at low density [39].

Our results help establish optimal conditions for making sensitive responsive gels using dipolar colloid particles. The particles that we simulate could be used in rapidly settling gels of low particle volume fractions or in dipolar crystals, which are more robust than crystals formed by uniform spheres. The high sensitivity of dipolar interactions to the ionic concentration in dispersing media means that gels and crystals thus created would be highly responsive to changes in salt, pH, or concentration of ionic adsorbing species. This could allow the systems to be gelled and ungelled by adding a small volume of acidic, basic, salt, or surfactant solution. A variety of other environmentally sensitive smart materials could be fabricated from such structure-forming suspensions and can be simulated by the procedures presented here.

We thank the Department of Energy (DOE) for funding and Dr. Arun Yethiraj for helpful discussions.

[1] O. Cayre, V. N. Paunov, and O. D. Velev, J. Mater. Chem. **13**, 2445 (2003).
[2] C. J. Martinez, J. Liu, S. Rhodes, E. Luijten, E. Weeks, and J. A. Lewis, Langmuir **21**, 9978 (2005).
[3] W. B. Hu and D. Frenkel, Adv. Polym. Sci. **191**, 1 (2005).
[4] S. C. Glotzer, M. J. Solomon, and N. A. Kotov, AIChE J. **50**, 2978 (2004).
[5] K. Van Workum and J. F. Douglas, Phys. Rev. E **73**, 031502 (2006).
[6] E. V. Shevchenko, D. V. Talapin, N. A. Kotov, S. O. Brien, and C. B. Murray, Nature (London) **439**, 55 (2006).
[7] A. M. Kalsin, M. Fialkowski, M. Pasewski, S. K. Smoukov, K. J. M. Bishop, and B. A. Grzybowski, Science **312**, 420 (2006).
[8] Y. Xia, B. Gates, Y. Yin, and Y. Lu, Adv. Mater. (Weinheim, Ger.) **12**, 693 (2000).
[9] M. E. Leunissen, C. G. Christova, A. P. Hynninen, C. P. Royall, A. I. Campbell, A. Imhof, M. Dijkstra, R. Roij, and A. V. Blaaderen, Nature (London) **437**, 235 (2005).
[10] E. B. Mock, H. D. Bruyn, B. S. Hawkett, R. G. Gilbert, and C. F. Zukoski, Langmuir **22**, 4037 (2006).
[11] K. P. Velikov, C. G. Christova, R. P. A. Dullens, and A. V. Blaaderen, Science **296**, 106 (2002).
[12] M. Parthasarathy and D. J. Klingenberg, Mater. Sci. Eng., R. **17**, 57 (1996).
[13] O. J. Cayre, V. N. Paunov, and O. D. Velev, Chem. Commun. (Cambridge) **18**, 2296 (2003).
[14] K. Nakahama, H. Kawaguchi, and K. Fujimoto, Langmuir **16**, 7882 (2000).
[15] K. Fuzimoto, K. Nakahama, M. Shidara, and H. Kawaguchi, Langmuir **15**, 4630 (1999).
[16] C. E. Snyder, A. M. Yake, J. D. Feick, and D. Velegol, Langmuir **21**, 4813 (2005).
[17] A. M. Yake, R. A. Panella, C. E. Snyder, and D. Velegol, Langmuir **22**, 9135 (2006).
[18] L. Hong, S. Jiang, and S. Granick, Langmuir **22**, 9495 (2006).
[19] A. P. Hynninen and M. Dijkstra, Phys. Rev. Lett. **94**, 138303 (2005).
[20] B. Groh and S. Dietrich, Phys. Rev. E **63**, 021203 (2001).
[21] B. Groh and S. Dietrich, Phys. Rev. E **53**, 2509 (1996).
[22] R. Blaak, M. A. Miller, and J. P. Hansen, Europhys. Lett. **78**, 26002 (2007).
[23] A. G. Zilman and S. A. Safran, Phys. Rev. E **66**, 051107 (2002).
[24] B. J. Alder and T. E. Wainwright, J. Chem. Phys. **31**, 459 (1959).
[25] D. C. Rapaport, J. Chem. Phys. **71**, 3299 (1979).
[26] A. Bellemans, J. Orban, and D. V. Belle, Mol. Phys. **39**, 781 (1980).
[27] H. C. Anderson, J. Chem. Phys. **72**, 2384 (1980).
[28] H. S. Gulati and C. K. Hall, J. Chem. Phys. **107**, 3930 (1997).
[29] Y. Zhou, C. K. Hall, and M. Karplus, Phys. Rev. Lett. **77**, 2822 (1996).
[30] A. J. Schultz, C. K. Hall, and J. Genzer, J. Chem. Phys. **120**, 2049 (2004).
[31] R. P. Sear, Phys. Rev. Lett. **76**, 2310 (1996).
[32] P. J. Camp, J. C. Shelley, and G. N. Patey, Phys. Rev. Lett. **84**, 115 (2000).
[33] P. J. Steinhardt, D. R. Nelson, and M. Ronchetti, Phys. Rev. Lett. **47**, 1297 (1981).
[34] Z. Li and C. K. Hall, Langmuir **20**, 8559 (2004).
[35] J. M. Caillol, J. Chem. Phys. **98**, 9835 (1993).
[36] P. R. Ten Wolde and D. Frenkel, Science **277**, 1975 (1997).
[37] S. Klapp and F. Forstmann, J. Chem. Phys. **106**, 9742 (1997).
[38] S. Klapp and F. Forstmann, Phys. Rev. E **60**, 3183 (1999).
[39] See EPAPS Document No. E-PLEEE8-77-059803 for supplementary movie showing self assembly of dipolar colloid particles from initial random configuration to final body-centred tetragonal (BCT) structure. For more information on EPAPS, see http://www.aip.org/pubservs/epaps.html